Eur Biophys J (2007) 36:113–120
DOI 10.1007/s00249-006-0112-4

ARTICLE

Changes induced by hyperosmotic mannitol in cerebral endothelial cells: an atomic force microscopic study

Zoltán Bálint · István A. Krizbai · Imola Wilhelm · Attila E. Farkas · Árpád Párducz · Zsolt Szegletes · György Váró

Received: 18 May 2006 / Revised: 20 September 2006 / Accepted: 10 October 2006 / Published online: 8 November 2006

Abstract Understanding the reaction of living cells in response to different extracellular stimuli, such as hyperosmotic stress, is of primordial importance. Mannitol, a cell-impermeable non-toxic alcohol, has been used successfully for reversible opening of the blood–brain barrier in hyperosmotic concentrations. In this study we analyzed the effect of hyperosmotic mannitol on the shape and surface structure of living cerebral endothelial cells by atomic force microscope imaging technique. Addition of clinically relevant concentrations of mannitol to the culture medium of the confluent cells induced a decrease of about 40% in the observed height of the cells. This change was consistent both at the nuclear and peripheral region of the cells. After mannitol treatment even a close examination of the contact surface between the cells did not reveal gap between them. We could observe the appearance of surface protrusions of about 100 nm. By force measurements the elasticity of the cells were estimated. While the Young's modulus of the control cells appeared to be 8.04 ± 0.12 kPa, for the mannitol-treated cells it decreased to an estimated value of 0.93 ± 0.04 kPa which points to large structural changes inside the cell.

Keywords Blood–brain barrier · Cell imaging · Cytoskeleton · Force measurement · Young's modulus

Z. Bálint · I. A. Krizbai · I. Wilhelm · A. E. Farkas · Á. Párducz · Z. Szegletes · G. Váró (✉)
Institute of Biophysics, Biological Research Center of the Hungarian Academy of Sciences,
Temesvari krt 62, Szeged 6726, Hungary
e-mail: varo@nucleus.szbk.u-szeged.hu

Introduction

Since the invention of the atomic force microscope (AFM) in 1986 (Binnig et al. 1986), it became a very important tool in the field of biology (Butt et al. 1990; Engel 1991). Besides the classical methods developed for electron microscopy, such as cell fixation with glutaraldehyde or paraformaldehyde (Moloney et al. 2004), the study of the living cells became possible (Pesen and Hoh 2005a, b; Dufrene 2003). The use of AFM opened the possibility to study directly the effect of extracellular stimuli and the action of different drugs on living cells.

Besides investigations of the surface and submembranous structures of living cells, AFM proved to be a useful tool in the study of spatial and temporal changes of the mechanical properties of different cell types (Hassan et al. 1998; Vinckier and Semenza 1998; Mathur et al. 2001; Sato et al. 2004). Furthermore, different aspects of cellular function such as cell growth on different surfaces (Chung et al. 2003; Domke et al. 2000), volume changes induced by Ca^{2+} depletion (Quist et al. 2000) or drug administration (Rotsch and Radmacher 2000) have been studied as well. At a higher resolution AFM is a unique imaging tool for visualizing the cytoskeletal organization of the cells (Le Grimellec et al. 1998; Mahaffy et al. 2004; Berdyyeva et al. 2005; Pesen and Hoh 2005a, b; Sharma et al. 2005).

Force measurements on the surface of the cells have revealed the elastic properties of different cells and cell structures (Vinckier and Semenza 1998; Sato et al. 2004; Wojcikiewicz et al. 2004; Sharma et al. 2005). Force measurements on the surface of a membrane-bound protein, with chemically coated

cantilevers resulted new information about the binding force between proteins (Ludwig et al. 1999; Pfister et al. 2005). Atomic force microscopy made possible even the measurement of forces involved in membrane protein anchoring and folding (Oesterhelt et al. 2000).

A broad range of different cell types were successfully investigated by AFM including endothelial cells (ECs) (Oberleithner et al. 2003; Kienberger et al. 2003; Pesen and Hoh 2005a), platelets (Radmacher et al. 1996), epithelial cells (Sharma et al. 2005), osteoblasts (Domke et al. 2000). One of the most intensively studied cell type with AFM is the EC. The vast majority of the studies were performed on human umbilical vein endothelial cells (HUVECs): effect of drugs such as aldosterone (Oberleithner et al. 2003; Oberleithner et al. 2004), mechanical characteristics (Mathur et al. 2001; Sato et al. 2004), single molecule-binding events (Pfister et al. 2005), growth rate (Chung et al. 2003), cell–cell interactions (Zhang et al. 2003) of these cells have been studied. Pulmonary microvascular ECs were also observed, focusing mainly on cytoskeletal elements (Pesen and Hoh 2005a, b). Cultured rat hepatic sinusoidal ECs were studied by AFM after drying the cells (Braet et al. 1997).

Much less is known about cerebral endothelial cells (CECs). These cells form the basis of the blood–brain barrier (BBB), which restricts the free movement of the substances between blood and neural tissue. While the BBB is indispensable for the normal function of the brain, it can be an impediment for the chemical treatment of diseases of the central nervous system. Attempts have been made to overcome the limited access of drugs by linking the active compound to a carrier (Pardridge 2002). An alternative possibility is the reversible opening of the BBB. High concentration of mannitol, a cell-impermeable non-toxic alcohol, has been successfully used for this purpose both experimentally and clinically, although the mechanism of osmotic disruption is not well understood (Rappoport et al. 2000; Neuwelt et al. 1991; Kroll and Neuwelt 1998; Doolitle et al. 2000). It has been shown that mannitol induces a reversible phosphorylation of β-catenin, a protein of the intercellular junctional complex in CECs (Farkas et al. 2005), which might contribute to the BBB opening. However, further information is needed about the effect of mannitol on CECs.

In the present study the effect of the hyperosmotic mannitol on the cerebral vascular endothelial cells was investigated by atomic force microscopy, to get a better understanding of its mechanism of action.

Materials and methods

Cell culture

GP8 rat brain endothelial cells (Greenwood et al. 1996) were cultured in 3.5 cm diameter Petri dishes (Falcon) coated with rat tail collagen in DMEM/F12 (Dulbecco's Modified Eagles Medium with F12 salt, from Sigma, a medium with physiological concentrations of inorganic salts, amino acids, vitamins, D-Glucose (3.15 g/l), HEPES, phenol red.) supplemented with 12% plasma derived serum (PDS, First Link, UK) at 37°C in 5% CO_2. Cells were grown until confluency.

The experiments were conducted in serum-free conditions within 4 h after removing the cells from the culture environment, at a temperature about 31°C. During this period the cells preserved their viability (Quist et al. 2000; Pesen and Hoh 2005a, b). In the course of the experiment the medium was exchanged with the same solution, containing 0.55 M mannitol (Sigma).

Instrumentation, imaging

AFM measurements were performed with an Asylum MFP-3D head and Molecular Force Probe 3D controller (Asylum Research, Santa Barbara, CA, USA). The driver program MFP—3D Xop was written in IGOR Pro software (version 5.03, Wavemetrics, Lake Oswego, OR, USA). The gold coated, silicon nitride, rectangular cantilevers had a typical spring constant of 0.03 N/m and V shape tip with a radius about 30 nm (Bio-lever, BL-RC150 VB-C1, Olympus, Optical Co. ltd., Tokyo, Japan). The cantilevers were silanized by a standard procedure described elsewhere (Gergely et al. 2004). The silanized tips are strongly hydrophobic, hindering the tip–cell interaction. The procedure consists of vapor deposition of a mixture of 10 ml bicyclohexane, 1–4 drops of octaldecyltrichlorosilane and 4–8 drops of carbon tetrachloride. The tips were incubated overnight in a closed chamber together with the above mixture. The spring constant of the cantilever was determined by thermal calibration. Typically 256×256 point scans were taken with a scan speed of about 50 μm/s (scan rate 0.6 Hz), if not otherwise mentioned. The measurements were carried out in contact mode in fluid with an average loading force of less than 1 nN. Both the trace and retrace images were measured and compared. No difference could be observed between them. The thickness of the cells was estimated from the height profile calculated across the image. Only the relative height of the cell could be measured because between the confluent cells no

cell-free surface could be observed. By using not confluent cell cultures, where cell-free surface of the Petri dish could be observed, the real height of the cells was estimated to be about 2.5 μm, while the observed height of the confluent cell culture was only about 2 μm. This fact does not influence the observation, how the cell height changed, only the value of the relative change. During the whole measurement the cantilever position and the set point of the instrument was kept constant within 5%. This assures a constant reference zero level, which does not coincide with the cell-free surface of the Petri dish. Even so, the relative changes were recorded correctly. A relative thickness of the cell was calculated by averaging the height at around the highest point of the cell on a 5×5 μm^2 area (mentioned as over the nucleus) and midway between this point and the boundary of the cell, also on a 5×5 μm^2 area (mentioned as out of nucleus).

One complete experiment was as follows. The Petri dish with the cells placed in the AFM was let to equilibrate for 30 min. Several images (2–5 images) of the confluent cells were recorded. Without moving the sample and the AFM head, the medium in the Petri dish was carefully exchanged with a medium containing 0.55 M mannitol. After 1 h waiting period, to achieve a total equilibration of the cells, usually the new scan was shifted less than the size of one image; typically 5–10 μm. Therefore, the previously observed cells could be scanned and identified. All experiments were repeated minimum three times.

Transmission electron microscopy

Confluent cultures of CECs were fixed in 1% formaldehyde and 1% glutaraldehyde in 0.1 M phosphate buffer and postfixed in 0.1% osmium tetroxide in 0.1 M phosphate buffer. The fixed cells were dehydrated and embedded in Spurr resin. Thin sections were cut using a Leica ultramicrotome, contrasted with uranyl acetate and lead citrate and examined using a Zeiss 902 electron microscope (EM).

The evaluation of the Young's modulus

The force measurements were carried out with the same cantilever in triggered mode with the z piezo working in a closed loop. Force curves were recorded with a constant speed of 0.5 μm/s on the nuclear region of the ECs, both in normal and in mannitol-containing medium. At this region the force are at least effectuated by the hard surface of the Petri dish (Dimitriadis et al. 2002; Pesen and Hoh 2005a). Calibration force curves on flat, clear regions of the Petri dish were also measured. The measurements were effectuated with a 20 nm trigger, which meant a maximum loading force of about 0.6 nN; 5–10 force measurements on the same point were averaged and the error estimated. To calculate the Young's modulus of the cell the approaching part of the force curve was used to avoid the effect of the adhesive force between the tip and the membrane (Vinckier and Semenza 1998). The indentation, the difference between the deflections of the cantilever, detected on hard surface and on the cell, was calculated according to Vinckier and Semenza (1998).

To obtain the Young's modulus the theory based on the work of Hertz (1881) and Sneddon (1965) was used and further developed for different tip forms, used in the AFM technique (Dimitriadis et al. 2002; Mathur et al. 2001; Vinckier and Semenza 1998). The force as a function of indentation Δz, for a conical tip with opening angle α is described by the equation:

$$F(\Delta z) = \frac{2E^*}{\pi(tg(\alpha))}\Delta z^2 \quad (1)$$

where E^* is the relative Young's modulus:

$$\frac{1}{E^*} \approx \frac{1-\mu_m^2}{E_m} \quad (2)$$

E_m is the Young's modulus and μ_m is the Poisson ratio of the cell (Vinckier and Semenza 1998).

Results and discussion

Endothelial cells have a good resistance to external mechanical impacts, to withstand in vivo exposure to the blood flow, collision with blood cells. They are resistant to the imaging force of the AFM as well (Pesen and Hoh 2005a, b; Ohashi and Sato 2005).

To characterize the surface on which the cells were grown, we scanned the rat tail collagen coated Petri dish (not shown). The maximum surface roughness was less than 20 nm about 1% the height of the observed ECs. The surface shows a continuous coverage with several nanometer high fibrous structures, without any characteristic, large feature. These structures facilitate the attachment of the cells to the Petri dish surface.

The AFM imaging experiments were conducted after the cells were checked by phase contrast microscopy for confluency. Placing the Petri dish in the instrument, half an hour was allowed for thermal stabilization, before the measurements were started. This assured the stability and repeatability of the measurements by diminishing to almost zero the thermal shift

of the consecutive images. The AFM scan of 40×40 μm^2 generally shows 2–3 cells (Fig. 1a). The nuclear region and the boundary of the cells are well resolved. The observed maximum cell height was about 2 μm (Fig. 1b). The scan was done with an average constant loading force kept bellow 1 nN. This force was suitable not to damage the cell surface but to visualize the cytoskeletal structures right below the membrane, more visible on the deflection image (Fig. 1c). By analyzing the height profile of the image at different places, an average of 50–100 nm thickness resulted for the cytoskeletal structure. These structures showed linear and branched fibers as described earlier (Han et al. 2004).

After changing the medium to that of mannitol containing one, the previously imaged area could be located, as it can be seen by comparing Fig. 1a, d. The mannitol treated sample exhibited characteristic changes. On the 40×40 μm^2 scan the height profile (Fig. 1e) showed a marked decrease and the distance between the positions of the maximum height of the two cells increased with several micrometers (Fig. 1d, e). Beside the filamentous structure, observed on the earlier images, small protrusions covering the body of the cells appeared. Although the filamentous structure of the cytoskeleton seemed preserved, its configuration was changed as was observed by others (Pesen and Hoh 2005b) and the surface was covered with the protrusions. The size of the bumps was around 100 nm.

It had to be excluded the effect of other external conditions, which eventually could change (pH, temperature, etc.) and alter the results. To assure that the observed effects were real, not an artifact, the same experiment was repeated with the only change that from the second solution mannitol was missing (Fig. 2). The experiment was done exactly with the same timing and scanning parameters, and no change in the shape and size of the cells could be detected over several hours (compare Fig. 2a–c to Fig. 2d–f, respectively). This assured that the observed effects were induced solely by the mannitol addition.

The EM images (Fig. 3) give some additional information about the structural features of the protrusions. The higher electron density image, representing

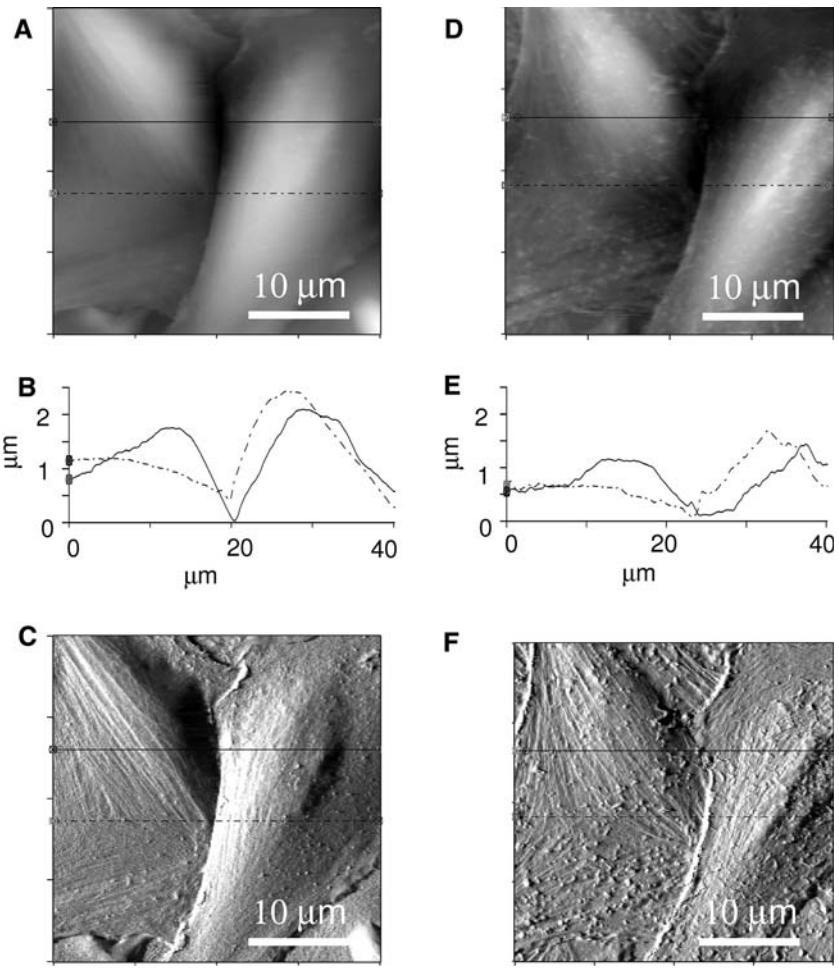

Fig. 1 The effect of the mannitol. AFM image of the endothelial cells with a scan size of 40×40 μm^2 height image of two cells in contact (**a**, **d**); height profile measured at the two corresponding lines on image (**b**, **e**); the deflection image showing the details of the cell surface (**c**, **f**). The images were taken before (**a**–**c**) and after mannitol treatment (**d**–**f**)

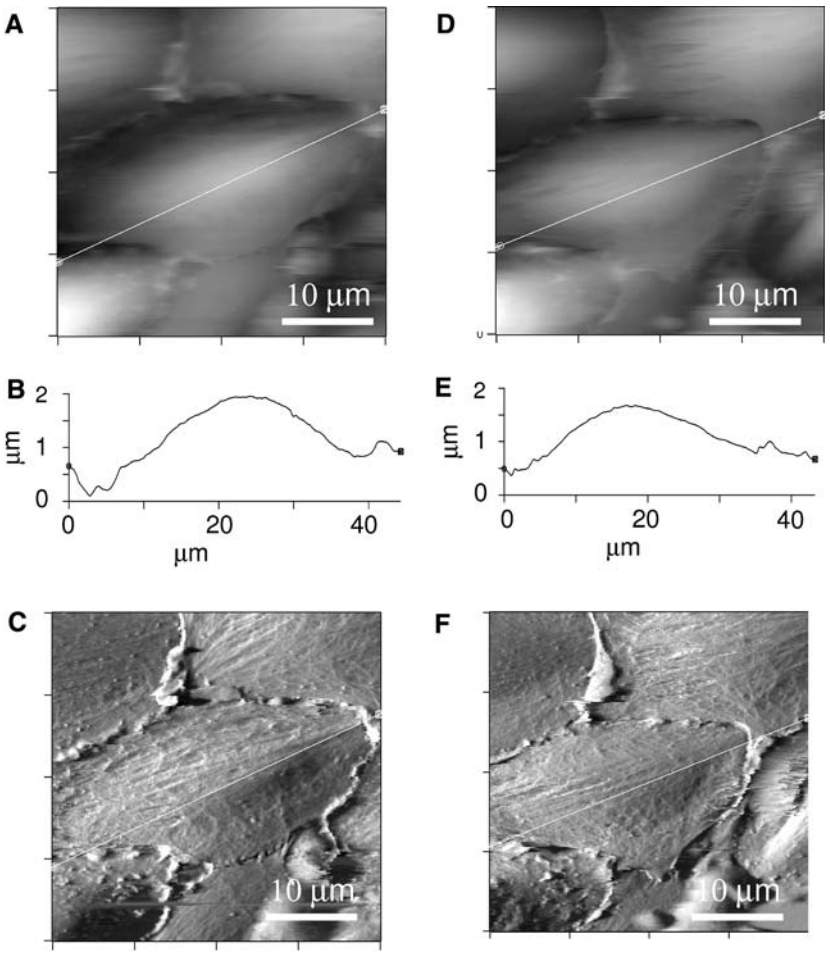

Fig. 2 The control experiment. AFM image of the endothelial cells with a scan size of 40×40 µm^2 height image of two cells in contact (**a**, **d**); height profile measured at the two corresponding lines on image (**b**, **e**); the deflection image showing the details of the cell surface (**c**, **f**). The images were taken before (**a**–**c**) and after changing the solution, but without mannitol (**d**–**f**). No significant change could be observed

the cell membrane, covers the bumps proving that the protrusions are part of the cell interior (See the inset of the Fig. 3b), with no specific structure observed at this resolution.

To prove the reversibility of the mannitol effect, it would have been good to continue the experiment by changing back the mannitol containing medium to that without it and observe the reversal of the changes, but even the sturdy ECs of the BBB were not stable for more than 4 h and so many AFM scanning, which would be needed for two solution changes. To overcome this difficulty a reversed experiment was performed. After the cells were grown to confluency, the original medium was exchanged to that containing mannitol. The cells in the Petri dish were scanned after half an hour equilibration in the AFM. They exhibited the characteristics of the mannitol treatment, reduced cell height and protrusions on the surface of the cell. By changing back the medium to its original composition, the cells showed an increase in height and the protrusions disappeared (not shown). These observations prove that the mannitol-induced changes are reversible.

To better characterize the osmotic effect of the mannitol, the change of the height of the cells was averaged over all the experiments conducted. Two separate places were chosen for the analyses, one over the nuclear area, which represents the highest point of the cell and one out of nuclear region, at halfway between the height maximum and the cell boundary. In both places the change of the height due to mannitol treatment showed an approximately 40% decrease (Fig. 4). Based on the EM images (Fig. 3), it can be considered that over the nucleus the larger part of the cell height is occupied by the nuclear material. Our result suggests that not only the cytoplasm of the cell suffers osmotic shrinkage, but also the interior of the nucleus is affected. The mannitol does not penetrate the cell, but osmotically drives the water out from the cell, decreasing the pressure in the cytoplasm. The excess pressure of the nucleus is equilibrated by water exclusion as well.

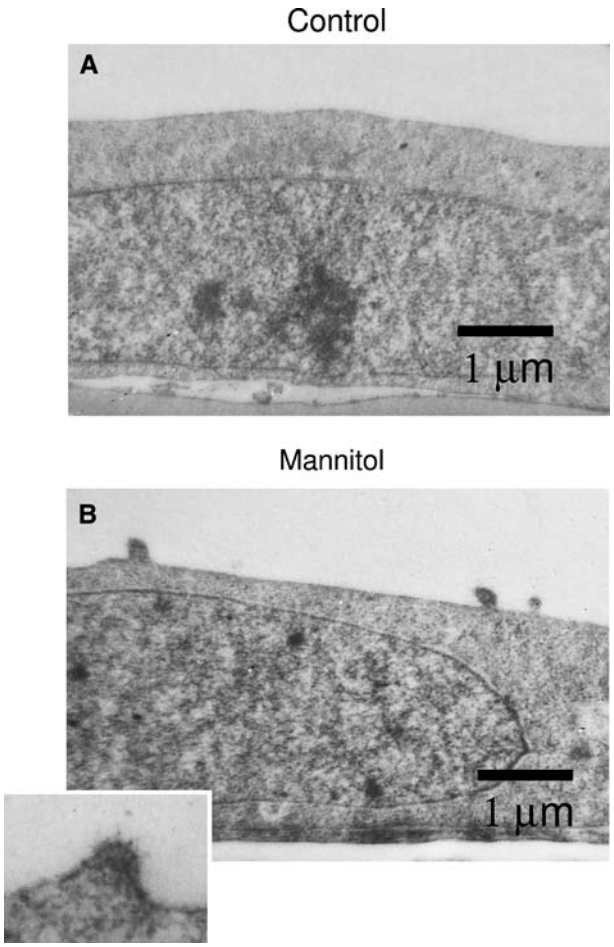

Fig. 3 Electron microscopic image of the section of a cell without mannitol treatment (**a**) and another one after mannitol treatment (**b**). The scale-bar represents 1 μm. The *inset* shows the enlarged image of a protrusion

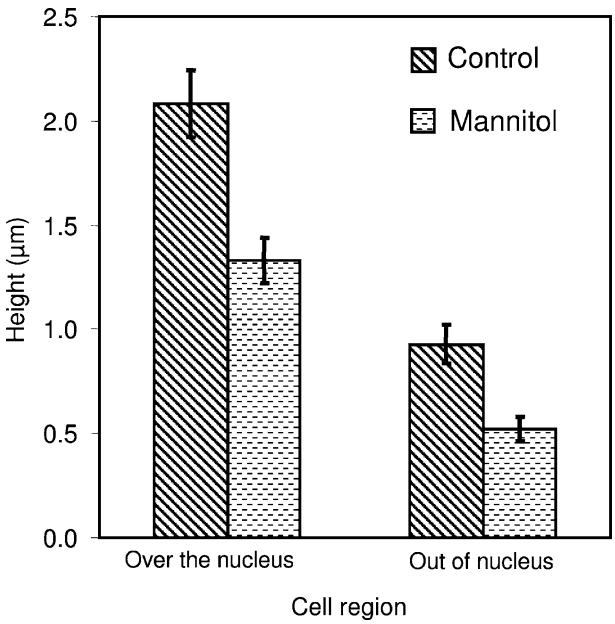

Fig. 4 The average observed thickness of the cells measured over the nucleus and at the peripherical region of the cell, in normal conditions and after mannitol treatment

Although after mannitol treatment the maximum height position of the two cells, presented on the figures, moved with about 2–3 μm, the close examination of the boundary of the cells in Fig. 1c, f does not reveal any rupture of the contact between them. CECs do not overlap, even when they are confluent (Mathur et al. 2001; Han et al. 2004). Any 2–3 μm discontinuity in the contact would make visible the collagen structure, which is not the case. The normal size cells are bound through four different junctions: tight junctions, adherence junctions, gap junctions and syndesmos (Dejana et al. 1995). The membranes by their surface tension close any path between the cells. After mannitol treatment the cells suffer an osmotic shock and lose from their volume, becoming slack. The loose membrane contact between the cells does not block the penetration of the molecules between the cell membranes.

To characterize the changes in the cell mechanical properties the Young's modulus was determined by force measurements over the nucleus of the cell, for the control and mannitol-treated cultures (Fig. 5a, curves C and M, respectively). As reference the hard surface of the Petri dish was measured (Fig. 5a, curve S). From these data the indentation of the cell membrane was calculated for both the control and mannitol-treated cells (Fig. 5b, curves C and M, respectively). As the figure shows, the indentation of the mannitol-treated membrane is much larger, compared to the control. Apparently the mannitol-treated membrane is much softer, which can be explained by the fact that the mannitol treatment removes a large part of the cell volume, but the surface remains constant.

The calculated Young's modulus, based on the theory mentioned in the Materials and methods, was 8.04 ± 0.12 kPa for the control and 0.93 ± 0.04 kPa for the mannitol-treated cells, if the tip angle was taken to be $\alpha = 45°$ and the Poisson ratio $\mu = 0.4$ (Mathur et al. 2001). The ratio between the two moduli is larger than 8, which means that the hyperosmotic stressed cells become much softer than the control ones. The value of the Young's modulus for the control cells is in good agreement with that calculated by others (Mathur et al. 2001). Although the exact value of the Young's modulus is model dependent, the dramatic change of its value after mannitol treatment points to important changes occurring deep inside the cell. These changes were not observed by the AFM study, which observes only structural changes close to the membrane surface of the cell.

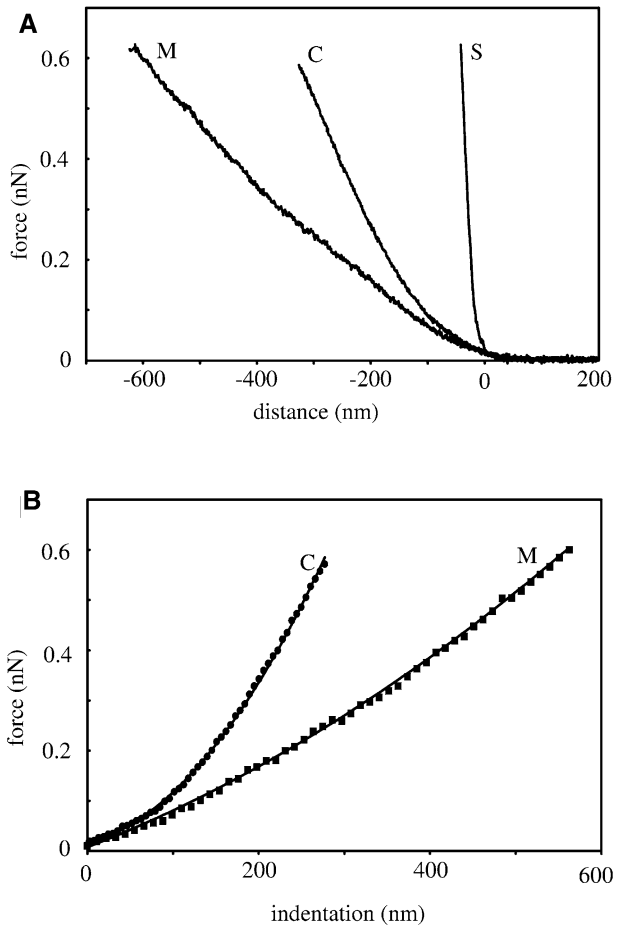

Fig. 5 Force curves on the Petri dish surface (*S*) and on endothelial cells before (*C*) and after (*M*) mannitol treatment. From the measured force versus distance curves (**a**) the force versus indentation curves were calculated (**b**, *points*) and the fits to the Hertz model are shown (**b**, *continuous lines*)

The changes observed by AFM might contribute to understand the effect of opening the BBB by mannitol. We have previously shown that mannitol treatment induces changes in the junctional complex at molecular level: Src kinase-mediated phosphorylation of beta-catenin and the disruption of the catenin–cadherin complex (Farkas et al. 2005). Osmotic stress-induced volume changes, observed in the above experiments, might also contribute to the permeability increase, especially as the molecules of the junctional complex are connected to the actin cytoskeleton. These observations predict that the opening of the BBB happens by the transient increase of the intercellular space between the ECs.

Acknowledgment We acknowledge the technical work of N.T.K Dung. We are grateful for the technical assistance provided by the German representatives of the Asylum Research and especially to Stefan Vinzelberg. This work was supported by the National Science Fund of Hungary OTKA T048706 and T037956 and partly Philip Morris Inc. USA.

References

Berdyyeva T, Woodworth CD, Sokolov I (2005) Visualization of cytoskeletal elements by the atomic force microscope. Ultramicroscopy 102:189–198

Binnig G, Quate CF, Gerber C (1986) Atomic force microscope. Phys Rev Lett 56:930–933

Braet F, deZanger R, Wisse E (1997) Drying cells for SEM, AFM and TEM by hexamethyldisilazane: a study on hepatic endothelial cells. J Microsc 186:84–87

Butt HJ, Wolff EK, Gould SAC, Northern BD, Peterson CM, Hansma PK (1990) Imaging cells with the atomic force microscope. J Struct Biol 105:54–61

Chung TW, Liu DZ, Wang SY, Wang SS (2003) Enhancement of the growth of human endothelial cells by surface roughness at nanometer scale. Biomaterials 24:4655–4661

Dejana E, Corada M, Lampugnani MG (1995) Endothelial cell-to-cell junctions. Faseb J 9:910–918

Dimitriadis EK, Horkay F, Maresca J, Kachar B, Chadwick RS (2002) Determination of elastic moduli of thin layers of soft material using the atomic force microscope. Biophys J 82:2798–2810

Domke J, Dannohl S, Parak WJ, Muller O, Aicher WK, Radmacher M (2000) Substrate dependent differences in morphology and elasticity of living osteoblasts investigated by atomic force microscopy. Colloids Surf B Biointerfaces 19:367–379

Doolitle ND, Miner ME, Hall WA, Siegal T, Jerome E, Osztie E, McAllister LD, Bubalo JS, Kraemer DF, Fortin D, Nixon R, Neuwelt EA (2000) Safety and efficacy of a multicenter study using intraarterial chemotherapy in conjunction with osmotic opening of the blood–brain barrier for the treatment of patients with malignant brain tumors. Cancer 88:637–647

Dufrene YF (2003) Recent progress in the application of atomic force microscopy imaging and force spectroscopy to microbiology. Curr Opin Microbiol 6:317–323

Engel HA (1991) Biological applications of scanning probe microscopes. Ann Rev Biophys Biophys Chem 20:79–108

Farkas A, Szatmári E, Orbók A, Wilhelm I, Wejszka K, Nagyõszi P, Hutamekalin P, Bauer H, Bauer HC, Traweger A, Krizbai IA (2005) Hyperosmotic mannitol induces Src kinase-dependent phosphorylation of beta-catenin in cerebral endothelial cells. J Neurosci Res 80:855–861

Gergely C, Bahi S, Szalontai B, Flores P, Schaaf P, Voegel JC, Cuisinier FJG (2004) Human serum albumin self-assambly on weak polyelectrolyte multilayer films structurally modified by pH changes. Langmuir 20:5575–5582

Greenwood J, Pryce G, Devin L, dos-Santos WL, Calder VL, Adamson P (1996) SV40 large T immortalised cell lines of the rat blood–brain and blood–retinal barriers retain their phenotypic and immunological characteristics. J Neuro immunol 71:51–63

Han D, Ma WY, Liao FL, Chen DY (2004) Intracellular structural changes under the stress of applied force at a nanometre range investigated by atomic force microscopy. Nanotechnology 15:120–126

Hassan EA, Heinz WF, Antonik MD, D'Costa NP, Nageswaran S, Schoenenberger CA, Hoh JH (1998) Relative microelastic mapping of living cells by atomic force microscopy. Biophys J 74:1564–1578

Hertz MG (1881) Uber die Beruhrung Fester Elastischer Korper. J Reine Angew Math 92:156–171

Kienberger F, Stroh CM, Kada G, Moser R, Baumgartner W, Pastushenko V, Rankl C, Schmidt U, Muller H, Orlova E, LeGrimellec C, Drenckhahn D, Blaas D, Hinterdorfer P (2003) Dynamic force microscopy imaging of native membranes. Ultramicroscopy 97:229–237

Kroll RA, Neuwelt EA (1998) Outwitting the blood–brain barrier for therapeutic purposes: osmotic opening and other means. Neurosurgery 42:1083–1099

Le Grimellec C, Lesniewska E, Giocondi MC, Finot E, Vie V, Goudonnet JP (1998) Imaging of the surface of living cells by low-force contact-mode atomic force microscopy. Biophys J 75:695–703

Ludwig M, Rief M, Schmidt L, Li H, Oesterhelt F, Gautel M, Gaub HE (1999) AFM, a tool for single-molecule experiments. Appl Phys A Mater Sci Process 68:173–176

Mahaffy RE, Park S, Gerde E, Kas J, Shih CK (2004) Quantitative analysis of the viscoelastic properties of thin regions of fibroblasts using atomic force microscopy. Biophys J 86:1777–1793

Mathur AB, Collinsworth AM, Reichert WM, Kraus WE, Truskey GA (2001) Endothelial, cardiac muscle and skeletal muscle exhibit different viscous and elastic properties as determined by atomic force microscopy. J Biomech 34:1545–1553

Moloney M, McDonnell L, O'Shea H (2004) Atomic force microscopy of BHK-21 cells: an investigation of cell fixation techniques. Ultramicroscopy 100:153–161

Neuwelt EA, Goldman DL, Dahlborg SA, Crossen J, Ramsey F, Roman-Goldstein S, Brazile R, Dana B (1991) Primary CNS lymphoma treated with osmotic blood–brain barrier disruption: prolonged survival and preservation of cognitive function. J Clin Oncol 9:1580–1590

Oberleithner H, Ludwig T, Riethmuller C, Hillebrand U, Albermann L, Schafer C, Shahin V, Schillers H (2004) Human endothelium: target for aldosterone. Hypertension 43:952–956

Oberleithner H, Schneider SW, Albermann L, Hillebrand U, Ludwig T, Riethmuller C, Shahin V, Schafer C, Schillers H (2003) Endothelial cell swelling by aldosterone. J Membr Biol 196:163–172

Oesterhelt F, Oesterhelt D, Pfeiffer M, Engel HA, Gaub HE, Muller DJ (2000) Unfolding pathways of individual bacteriorhodopsins. Science 288:143–146

Ohashi T, Sato M (2005) Remodeling of vascular endothelial cells exposed to fluid shear stress: experimental and numerical approach. Fluid Dyn Res 37:40–59

Pardridge WM (2002) Drug and gene delivery to brain: the vascular rout. Neuron 36:555–558

Pesen D, Hoh JH (2005a) Micromechanical architecture of the endothelial cell cortex. Biophys J 88:670–679

Pesen D, Hoh JH (2005b) Modes of remodeling in the cortical cytoskeleton of vascular endothelial cells. Febs Lett 579:473–476

Pfister G, Stroh CM, Perschinka H, Kind M, Knoflach M, Hinterdorfer P, Wick G (2005) Detection of HSP60 on the membrane surface of stressed human endothelial cells by atomic force and confocal microscopy. J Cell Sci 118:1587–1594

Quist AP, Rhee SK, Lin H, Lal R (2000) Physiological role of gap-junctional hemichannels: extracellular calcium-dependent isosmotic volume regulation. J Cell Biol 148:1063–1074

Radmacher M, Fritz M, Kacher CM, Cleveland JP, Hansma PK (1996) Measuring the viscoelastic properties of human platlets with the atomic force microscope. Biophys J 70:556–567

Rappoport SI, Fredeicks WR, Ohno K, Pettigrew KD (2000) Quantitative aspects of reversible osmotic opening of blood–brain barrier. Am J Phys 238:R421–431

Rotsch C, Radmacher M (2000) Drug-induced changes of cytoskeletal structure and mechanics in fibroblasts: an atomic force microscopy study. Biophys J 78:520–535

Sato H, Kataoka N, Kajiya F, Katano M, Takigawa T, Masuda T (2004) Kinetic study on the elastic change of vascular endothelial cells on collagen matrices by atomic force microscopy. Colloids Surf B Biointerfaces 34:141–146

Sharma A, Anderson K, Muller DJ (2005) Actin microridges characterized by laser scanning confocal and atomic force microscopy. Febs Lett 579:2001–2008

Sneddon IN (1965) The relation between load and penetration in the axisymmetric Boussinesq problem for a punch of arbitrary profile. Int J Engr Sci 3:47–57

Vinckier A, Semenza G (1998) Measuring elasticity of biological materials by atomic force microscopy. Febs Lett 430:12–16

Wojcikiewicz EP, Zhang X, Moy VT (2004) Force and compliance measurements on living cells using atomic force microscopy (AFM). Biol Proced Online 6:1–9

Zhang X, Chen A, De Leon D, Li H, Noiri E, Moy VT, Goligorsky MS (2003) Atomic force microscopy measurement of leukocyte-endothelial interaction. Am J Physiol Heart Circ Physiol 286:H359–367